

Dynamics of Weyl quasiparticles emerged in an optical lattice

Zhi Li,^{1,2} Huai-Qiang Wang,¹ Dan-Wei Zhang,² Shi-Liang Zhu,^{1,3,*} and Ding-Yu Xing^{1,4,†}

¹National Laboratory of Solid State Microstructures and School of Physics, Nanjing University, Nanjing 210093, China

²Guangdong Provincial Key Laboratory of Quantum Engineering and Quantum Materials, SPTE, South China Normal University, Guangzhou 510006, China

³Synergetic Innovation Center of Quantum Information and Quantum Physics, University of Science and Technology of China, Hefei, Anhui 230026, China

⁴Collaborative Innovation Center of Advanced Microstructures, Nanjing University, Nanjing 210093, China

(Dated: July 7, 2021)

We investigate the dynamics of the Weyl quasiparticles emerged in an optical lattice where the topological Weyl semimetal and trivial band insulator phases can be adjusted with the on-site energy. The evolution of the density distribution is demonstrated to have an anomalous velocity in Weyl semimetal but a steady *Zitterbewegung* effect in the band insulator. Our analysis demonstrates that the chirality of the system can be directly determined from the positions of the atomic center-of-mass. Furthermore, the amplitude and the period of the relativistic *Zitterbewegung* oscillations are shown to be observable with the time-of-flight experiments.

PACS numbers: 67.85.-d, 03.65.Vf, 03.75.Kk

I. INTRODUCTION

Weyl equation, first proposed by Hermann Weyl, is a relativistic wave equation to describe massless spin-1/2 particles in quantum field theory [1]. But such fermions (so-called Weyl fermions) have not been observed as fundamental particles in nature [2]. Recently, it was demonstrated that a Weyl fermion can emerge as a quasiparticle in condensed matter [3–5] or photonic crystals [6, 7]-Weyl semimetal (WSM). In WSM, two linear dispersion bands in three-dimensional (3D) momentum space intersect as a single degenerate point—the Weyl point, which is a monopole of Berry flux with topological charge defined by the Chern number. Many intriguing features of the WSM, such as the topologically protected Fermi arc on the surface and the Weyl points in the bulk, have been experimentally observed in condensed matter [8, 9] or photonic crystals [10]; however, the fundamental dynamics of the Weyl equation is hard to detect in such systems. On the other hand, it was recently proposed that the WSM can be realized with ultracold atoms loaded into a tunable cubic lattice [11–14]. This provides a versatile platform to study the dynamics of the Weyl quasiparticles, which has not yet been investigated.

In this paper, we exploit the dynamics of the Weyl quasiparticles emerged in an optical lattice, which is otherwise difficult to do in condensed matter systems. We consider a Gaussian wave packet which is formed by a harmonic trap and initially placed at a fixed Weyl point in the optical lattice. After releasing the trap, the atoms would start expanding in the 3D Weyl lattice, and hence the dynamics of the atoms, which is described by the Weyl equation, can be exploited with the time-of-

flight (TOF) experiments (hereafter the “TOF” denotes the evolution experiments of atomic gases in the Weyl lattice rather than the traditional TOF where the lattice potential is also released.). We calculate the time-dependent density profiles and find that the 3D Gaussian wave packet in WSM gradually evolves into a two-layer spherical shell structure because of the interference of the positive and negative energy states. We then demonstrate that the topological Chern number and the chirality of the system can be directly determined from the time-dependent position of the center-of-mass (PCM). Furthermore, we show that the amplitude and the period of the relativistic *Zitterbewegung* (ZB) in the trivial band insulator (BI) are sufficiently large to be observable. Notably, the topological Chern number and ZB have not yet been directly observed in condensed matter systems. Since the density profiles can be readily observed with TOF experiments, our work may stimulate the experimental study of the dynamics of the Weyl fermions in optical lattices.

The paper is organized as follows. In Sec. II, we review the scheme proposed in Ref.[11] for realizing the Weyl quasiparticle with cold atomic gases in optical lattice. In Sec. III, we investigate and discuss the dynamics of Weyl quasiparticles in 3D optical lattices. We give a brief summary in section IV. The split-operator method used in this work and some computational details for topological invariants are listed in Appendix.

II. MODEL

The model under consideration is a cubic lattice with phase engineered hopping along x - and z -directions, which possesses Weyl points in the momentum space.

*Electronic address: slzhu@nju.edu.cn

†Electronic address: dyxing@nju.edu.cn

The tight-binding Hamiltonian is given by the form [11]

$$\hat{H} = - \sum_{m,n,l} \{ [J_x e^{-i\Phi_{m,n,l}} \hat{a}_{m+1,n,l}^\dagger + J_z e^{-i\Phi_{m,n,l}} \hat{a}_{m,n,l+1}^\dagger + J_y \hat{a}_{m,n+1,l}^\dagger + (-1)^{(m+n-1)} \frac{\varepsilon}{2} \hat{a}_{m,n,l}^\dagger] \hat{a}_{m,n,l} + \text{H.c.} \}, \quad (1)$$

where $J_{x,y,z}$ denote the tunnelling amplitudes, $\hat{a}_{m,n,l}^\dagger$ ($\hat{a}_{m,n,l}$) is the creation (annihilation) operator on the site (m, n, l) , and $\Phi_{m,n,l} = m\Phi_x + n\Phi_y + l\Phi_z$ are the nontrivial hopping phases. As shown in Fig. 1(a)(b), the lattice is a stacking of 2D Harper-Hofstadter lattice which has already been realized experimentally [15–17], and the z -direction hopping has phase 0 (π) for $m+n$ even (odd). The lattice has two sublattices (A-B) giving rise to pseudospin. The on-site energy is $\varepsilon/2$ ($-\varepsilon/2$) for $m+n$ odd (even), which is the key parameter for manipulating the topological phase transition of the system. The positions of the sites can be expressed as $\mathbf{R}_{m,n,l} = m\mathbf{a}_1 + n\mathbf{a}_2 + l\mathbf{a}_3$, where m, n and l are integers, and $\mathbf{a}_1 = (a, 0, 0)$, $\mathbf{a}_2 = (0, a, 0)$ and $\mathbf{a}_3 = (0, 0, a)$ (hereafter we set the lattice spacing $a = 1$). By introducing Fourier transform $\hat{a}_{m,n,l}^\dagger = \sum_{\mathbf{k}} e^{i\mathbf{k}\cdot\mathbf{R}_{m,n,l}} \hat{a}_{\mathbf{k}}^\dagger$, where $\mathbf{k} = (k_x, k_y, k_z)$ is the Bloch wave vector, we obtain the Hamiltonian in quasimomentum representation given by

$$H_{\mathbf{k}} = -2J_y \cos k_y \sigma_x - 2J_x \sin k_x \sigma_y + (\varepsilon + 2J_z \cos k_z) \sigma_z, \quad (2)$$

where the Pauli matrices σ_j ($j = x, y, z$) are pseudospins describing A and B sublattices of the system. The WSM is usually realized when the time-reversal symmetry or inversion symmetry is broken. The \mathbf{k} -space Hamiltonian in Eq. (2) has time reversal symmetry, $H(\mathbf{k})^* = H(-\mathbf{k})$, but inversion symmetry is broken here because $\sigma_x H(\mathbf{k}) \sigma_x \neq H(-\mathbf{k})$. Nevertheless, since the quasiparticles' evolution we obtained is entirely derived from the low-energy effective Hamiltonian and depends totally on the structure and topological property of Weyl points, these results are therefore also valid for the case of WSM with broken time reversal symmetry which has the same spectrum. The energy spectrum of the Bloch bands is given by

$$E_{\mathbf{k}} = \pm \sqrt{4J_x^2 \sin^2 k_x + 4J_y^2 \cos^2 k_y + (\varepsilon + 2J_z \cos k_z)^2}, \quad (3)$$

which is plotted in Figs. 1(c-e) for typical values of ε .

The system is a WSM phase for $\varepsilon < |\varepsilon_c|$ and a band insulator for $\varepsilon > |\varepsilon_c|$ with the critical points $\varepsilon_c = \pm 2J_z$. In WSM phase, the energy spectra touch at four Weyl points (two pairs) in the first Brillouin zone at $\mathbf{W}_\pm = (0, \pm \frac{\pi}{2}, \pm \arccos \frac{\varepsilon}{2J_z})$. By making ε large enough ($\varepsilon > |\varepsilon_c|$), the Weyl points with opposite chiralities can be driven to annihilate at $\mathbf{M} = (0, \pm \frac{\pi}{2}, 0)$ for $\varepsilon_c = -2J_z$ or at the edge of BZ for $\varepsilon_c = 2J_z$. Without loss of generality, we only consider the case of $\varepsilon_c = -2J_z$, and set $\mathbf{k} =$

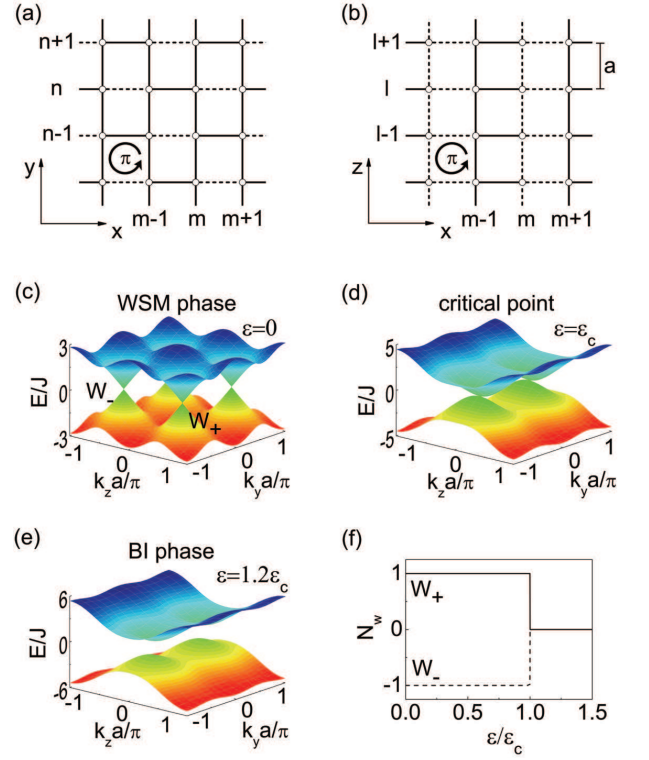


FIG. 1: (Color online). (a,b) Schematic view of the tight-binding model described in Eq. (1). Solid and dash lines depict hopping with acquired phase 0 and π , respectively. The dispersion relations in the $k_x = 0$ cross-section for (c) WSM phase with $\varepsilon = 0$, (d) critical point $\varepsilon = \varepsilon_c$ and (e) BI phase with $\varepsilon = 1.2\varepsilon_c$. (f) The winding number N_w as a function of ε .

$\mathbf{W}_\pm + \mathbf{q}$, where $\mathbf{q} = (q_x, q_y, q_z)$ is the displacement vector measured from the Weyl point \mathbf{W}_\pm in momentum space. By expanding the quasi-momentum \mathbf{k} at \mathbf{W}_\pm , the low-energy effective spectrum can be obtained as

$$E_{\mathbf{q}} = \pm \sqrt{\alpha_x^2 v_x^2 q_x^2 + \alpha_y^2 v_y^2 q_y^2 + (\Delta + \alpha_z v_z q_z + \frac{\hbar^2 q_z^2}{2m^*})^2} \quad (4)$$

with $\alpha_{x,y,z} = \pm 1$ and $v_{x,y,z} = (2J_x, 2J_y, \sqrt{4J_z^2 - \varepsilon^2})/\hbar$, $\Delta = 0$ and $m^* = 1/\varepsilon$ for the WSM phase; $v_{x,y,z} = (2J_x, 2J_y, 0)/\hbar$, $\hbar\Delta = \varepsilon - \varepsilon_c$ and $m^* = 1/\varepsilon_c$ for the BI phase. For simplicity, throughout we set $J_{x,y,z} = J = 1$ as the energy unit. In the regime of WSM phase far away from the critical point ε_c , the quadratic term can be neglected. Then $E_{\mathbf{q}}$ exhibits a typical Weyl point spectrum $E_{\mathbf{q}} = \pm \sqrt{v_x^2 q_x^2 + v_y^2 q_y^2 + v_z^2 q_z^2}$. The Fermi velocities in the three orthogonal directions are equal for $\varepsilon = 0$, so we denote it as $v_{x,y,z} = v_F$. However, when the system is very close to the phase transition point, the value of v_z tends to zero, the $v_z q_z$ and the $\hbar^2 q_z^2/(2m^*)$ terms in Eq. (4) are of the same order. The quadratic term cannot be neglected. At the critical point, as $v_z = 0$ exactly, the linear term disappears and the quadratic term becomes dominant. This causes the hybrid spectrum

$E_{\mathbf{q}} = \pm \sqrt{v_x^2 q_x^2 + v_y^2 q_y^2 + (\Delta + \frac{\hbar^2 q_z^2}{2m^*})^2}$, which is linear in x - and y -direction but quadratic in z -direction.

The wave function for the low-energy quasiparticles around the Weyl point satisfies the equation of motion

$$i\hbar\partial_t\Psi = \hat{H}_{\text{eff}}\Psi, \quad (5)$$

where the effective Hamiltonian

$$H_{\text{eff}} = \vec{\sigma} \cdot \vec{g} \quad (6)$$

with

$$\vec{g} = (\alpha_y v_y q_y, \alpha_x v_x q_x, \Delta + \alpha_z v_z q_z + \frac{\hbar^2 q_z^2}{2m^*}). \quad (7)$$

It is a 3D relativistic Hamiltonian which is valid for describing the dynamics of the system in the whole process of the phase transition from a Weyl semimetallic to a band insulating phase. Notably, the 2D atomic Dirac fermions and the related topological phase transition [18–23] have been experimentally observed by several groups [24–26]. The system can be characterized by the winding number defined by [27]

$$N_w = \frac{1}{8\pi} \epsilon_{ijk} \int_{\Sigma_2} dS^k \hat{g} \cdot \left(\frac{\partial \hat{g}}{\partial q_i} \times \frac{\partial \hat{g}}{\partial q_j} \right), \quad (8)$$

where the unit vector $\hat{g} = \vec{g}/|\vec{g}|$, and dS^k is an area element of the sphere Σ_2 around the singular point in the momentum space. The winding number N_w versus ϵ for Weyl points with opposite chiralities are plotted in Fig. 1(f). It is clear that $N_w = \pm 1$ in the WSM phase and zero in the BI phase.

III. THE EVOLUTION OF WAVE-PACKET DYNAMICS

Realization of the optical Weyl lattice with ultracold atoms will open a new frontier of research in Weyl physics, especially one can exploit the dynamics of the particles described by the Weyl equation, which might be hard to study in a condensed matter system. Here we consider a Bose-Einstein condensation (BEC, or a cold atomic ensemble) initially described by a 3D Gaussian wave packet

$$|\Psi\rangle = (1/\sqrt{2\pi})^3 \int d^3\mathbf{q} [(L/\sqrt{\pi})^{\frac{3}{2}} e^{-\frac{1}{2}L^2\mathbf{q}^2} e^{i\mathbf{q}\mathbf{r}}] |\Phi\rangle, \quad (9)$$

with the width L . The initial spinor state is chosen as $|\Phi\rangle = (\frac{1}{\sqrt{3-\sqrt{3}}}, \frac{1}{\sqrt{3+\sqrt{3}}} e^{i\frac{\pi}{4}})$, in which $\langle\Phi|\sigma_j|\Phi\rangle = 1/\sqrt{3}$ ($j = x, y, z$). The Gaussian wave packet (9) can be formed by applying an additional 3D isotropic harmonic trap on the Weyl lattices, and then move the harmonic potential with a velocity $\hbar\mathbf{W}_{\pm}/m_A$ with m_A being the atomic mass to place the BEC at the Weyl point \mathbf{W}_{\pm} . In real space, such wave packet is also a Gaussian shape

and can be written as $|\Psi(\mathbf{r})\rangle = (1/\pi L^2)^{3/4} \exp(i\mathbf{W}_{\pm} \cdot \mathbf{r}) \exp(-r^2/2L^2)|\Phi\rangle$, where \mathbf{r} is the atomic position related to the center of the harmonic trap. One can show that the wave packet $|\Psi(\mathbf{r})\rangle$ in real space is related to $|\Psi\rangle$ in Eq. (9) (note that \mathbf{q} in Eq. (9) is the atom momentum related to the Weyl point \mathbf{W}_{\pm}) in momentum space with just a Fourier transform. After releasing the trap, the atoms would start expanding in the 3D Weyl lattice, and hence the dynamics of the atoms (such as the snapshots shown in Fig. 2 and the PCM in Figs. 3 and 4 below), which is described by the Weyl equation with the Hamiltonian determined by Eq. (6), can be exploited with the TOF experiments.

We calculate the time-dependent density profiles (which can be directly measured by the TOF experiments) by solving the Weyl equation with the standard split-operator method (see Appendix VI). The TOF snapshots of the $x = 0$, $y = 0$ and $z = 0$ cross-sections with a width of the wave packet $L = 10a$ are shown in Fig. 2(a) for the WSM phase and Fig. 2(b) for the BI phase. Since J can be tuned between $0.17 \sim 2.0$ kHz [15, 16], the time for $t = 15$ is about $0.6 \sim 7.1$ ms. In the WSM phase, the 3D Gaussian wave packet gradually evolves into a two-layer spherical shell structure. The pattern of the density profiles is determined by the interference of the positive and negative energy states. The destructive-interference shell between two constructive-interference spherical shell has a width of ten lattice sites for $t = 15$ and thus can be readily detected. The most significant features of the evolution of Weyl quasiparticles will be completely revealed when $t < 15$. Since Weyl quasiparticles are then moving away from the interference area of positive and negative energy states, the shape of wave packets will remain unchanged after time $t > 15$. In the BI phase, the density profiles exhibit the periodic oscillations in x - and y -axis direction, meanwhile the PCM of the atomic gas is confined in $z = 0$ plane. Since the oscillation of the PCM will become more salient after the wave function evolves for a longer time (here $t > 17$), we choose different period of time in Fig. 2 to reveal the features of Weyl and BI phases.

The PCM is a crucial quantity in the study of the dynamics of the atomic gas. It can be experimentally determined through TOF data, and in our theoretical calculation it can be obtained by the integral $\bar{\mathbf{r}}(t) = \int \mathbf{r}(t) |\Psi(\mathbf{r}(t))|^2 d^3\mathbf{r}$ with $|\Psi(\mathbf{r}(t))|^2$ being derived by the split-operator method. Alternatively, the PCM can be calculated analytically in the Heisenberg picture, where the position operator is given by

$$\hat{\mathbf{r}}(t) = e^{i\hat{H}_{\text{eff}}t/\hbar} \hat{\mathbf{r}}(0) e^{-i\hat{H}_{\text{eff}}t/\hbar}. \quad (10)$$

After inserting \hat{H}_{eff} into the expression, we obtain

$$\hat{\mathbf{r}}(t) = \hat{\mathbf{r}}(0) + \beta_{\mathbf{r}}t + \gamma_{\mathbf{r}}[\exp(2i\hat{H}_{\text{eff}}t/\hbar) - 1], \quad (11)$$

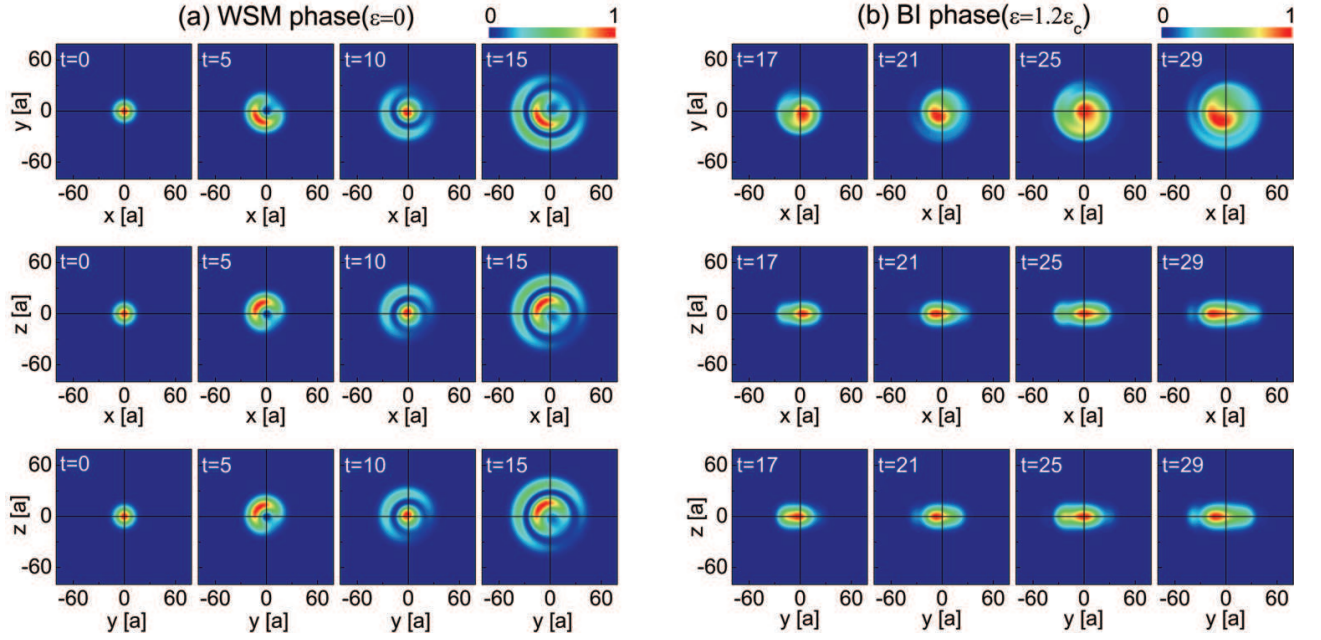


FIG. 2: (Color online). The TOF snapshots $|\Psi|^2$ with $L = 10a$ at different t (with the unit $a/v_F = \hbar/(2J)$) in $x(y, z) = 0$ cross-sections for (a) the WSM phase with $\epsilon = 0$ and (b) the BI phase with $\epsilon = 1.2\epsilon_c$. The value of the probability is rescaled from 0 to 1.

where the coefficients

$$\begin{aligned}
 \beta_{x,y} &= v_{x,y}^2 \hat{H}_{\text{eff}}^{-1} \hat{q}_{x,y}, \\
 \beta_z &= \hat{H}_{\text{eff}}^{-1} (\Delta + \alpha_z v_z \hat{q}_z + \frac{\hat{q}_z^2}{2m^*}) (\alpha_z v_z + \frac{\hat{q}_z}{m^*}), \\
 \gamma_{x,y} &= \frac{\hbar}{2iE_{\mathbf{q}}^2} (\alpha_{x,y} v_{x,y} \hat{H}_{\text{eff}} \sigma_{y,x} - v_{x,y}^2 \hat{q}_{x,y}), \\
 \gamma_z &= \frac{\hbar}{2iE_{\mathbf{q}}^2} [\hat{H}_{\text{eff}} \sigma_z - (\Delta + \alpha_z v_z \hat{q}_z + \frac{\hat{q}_z^2}{2m^*})] (\alpha_z v_z + \frac{\hat{q}_z}{m^*}).
 \end{aligned} \tag{12}$$

Hereafter $\hat{\mathbf{r}}$ and $\hat{\mathbf{q}}$ (\mathbf{r} and \mathbf{q}) are the coordinate and momentum operators (variables), respectively. By using the initial wave function in Eq. (9), the expectation values $\bar{x}(t)$, $\bar{y}(t)$ and $\bar{z}(t)$ can be obtained as

$$\begin{aligned}
 \bar{x}, \bar{y}(t) &= \frac{\alpha_{x,y}}{\sqrt{3}} \frac{L^3}{\pi^{\frac{3}{2}}} \iiint_{-\infty}^{+\infty} \{A_{x,y} t + \eta_{x,y} B_{x,y} [\cos(2E_{\mathbf{q}} t) \\
 &\quad - 1] + C_{x,y} \sin(2E_{\mathbf{q}} t)\} e^{-L^2 \mathbf{q}^2} d^3 \mathbf{q},
 \end{aligned} \tag{13}$$

$$\bar{z}(t) = \frac{\alpha_z}{\sqrt{3}} \frac{L^3}{\pi^{\frac{3}{2}}} \iiint_{-\infty}^{+\infty} [A_z t + C_z \sin(2E_{\mathbf{q}} t)] e^{-L^2 \mathbf{q}^2} d^3 \mathbf{q}, \tag{14}$$

where $\eta_x = -1$, $\eta_y = +1$, the other coefficients

$$\begin{cases}
 A_{x,y} = v_{x,y}^3 q_{x,y}^2 / E_{\mathbf{q}}^2 \\
 A_z = \frac{\hbar}{\alpha_z E_{\mathbf{q}}^2} (\alpha_z v_z + \frac{q_z}{m^*}) [(\Delta + \alpha_z v_z q_z + \frac{q_z^2}{2m^*})^2] \\
 B_{x,y} = \frac{\hbar}{2E_{\mathbf{q}}^2} (\Delta + q_z^2 / 2m^*) \\
 C_{x,y} = \frac{\hbar}{2E_{\mathbf{q}}^3} (v_{x,y} E_{\mathbf{q}}^2 - v_{x,y}^3 q_{x,y}^2) \\
 C_z = \frac{\hbar}{2\alpha_z E_{\mathbf{q}}^3} (\alpha_z v_z + \frac{q_z}{m^*}) [E_{\mathbf{q}}^2 - (\Delta + \alpha_z v_z q_z + \frac{q_z^2}{2m^*})^2]
 \end{cases} \tag{15}$$

Therefore, the PCM of the system can be straightforwardly obtained from Eqs. (13,14).

A. The PCM in the WSM phase

When $\epsilon \ll \epsilon_c$, $\Delta = 0$ and the terms related to m^* can be safely neglected, then the parameters $B_{x,y} = 0$, $A_{x,y,z} = v_{x,y,z}^3 q_{x,y,z}^2 / E_{\mathbf{q}}^2$ and $C_{x,y,z} = \frac{\hbar}{2E_{\mathbf{q}}^3} (v_{x,y,z} E_{\mathbf{q}}^2 - v_{x,y,z}^3 q_{x,y,z}^2)$. Therefore, the expressions of \bar{x} , \bar{y} and \bar{z} have the same form given by

$$\bar{r}(t) = \frac{\alpha_r}{\sqrt{3}} \frac{L^3}{\pi^{\frac{3}{2}}} \iiint_{-\infty}^{+\infty} \{A_r t + C_r \sin(2E_{\mathbf{q}} t)\} e^{-L^2 \mathbf{q}^2} d^3 \mathbf{q}. \tag{16}$$

The motion of PCM can be divided into two parts: the first term is a directed linear term with a constant anomalous velocity which plays a crucial role in the celebrated anomalous and spin Hall effects [28, 29], and the second term is a short-lived ZB term originating from the interference of positive and negative-energy states [30–37]. Furthermore, since the integrand in the expression is always positive, the signs of $\bar{r}(t)$ are completely determined by $\alpha_{x,y,z}$, therefore we have $\text{sgn}(\bar{x}\bar{y}\bar{z}) = \text{sgn}(\alpha_x\alpha_y\alpha_z)$, which implies that the sign of the PCM can be used to determine the chirality of each Weyl point.

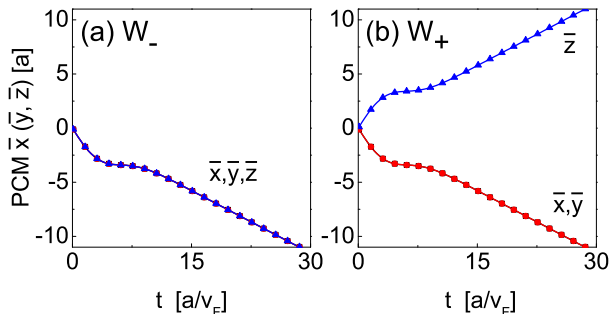


FIG. 3: (Color online). The expectation value $\bar{r}(t)$ for the atomic gas initially at the \mathbf{W}_{\pm} with $\varepsilon = 0$ and $L = 10a$. The lines are obtained from Eq. (16), and the symbols are derived by the split-operator method.

The Chern number of the valence band over a 2D sphere around a Weyl point equals the Weyl point's chirality, which can be proved as follows. The Berry curvature is given by $\Omega_{ij} = \epsilon_{abc}g_a\partial_i g_b\partial_j g_c/(2E_{\mathbf{q}}^3)$ [27], and for the Hamiltonian (6), we have

$$\mathbf{\Omega} = -\frac{\alpha_x\alpha_y\hbar^2v_xv_y}{2E_{\mathbf{q}}^3}(\alpha_zv_z\hbar q_x + \frac{\hbar^2q_zq_x}{m^*}, \quad (17)$$

$$\alpha_zv_z\hbar q_y + \frac{\hbar^2q_zq_y}{m^*}, \Delta + \alpha_zv_z\hbar q_z + \frac{\hbar^2q_z^2}{m^*}).$$

As for WSM, the Berry curvature of each Weyl point can be derived as $\mathbf{\Omega}_{\pm} = \mp \text{sgn}(\alpha_x\alpha_y\alpha_z)[\hbar^3v_xv_yv_z\mathbf{q}/2E_{\mathbf{q}}^3]$. After integrating the whole sphere surrounding a Weyl point, we derive the Chern number as $N_C = \text{sgn}(\alpha_x\alpha_y\alpha_z)$, and get the following relation

$$N_C = N_w = \text{sgn}(\bar{x}\bar{y}\bar{z}) = \text{sgn}(\alpha_x\alpha_y\alpha_z), \quad (18)$$

which is ± 1 for the Weyl points (see Appendix VI). The expectation values $\bar{r}(t)$ for the atomic gas initially located at the \mathbf{W}_{\pm} with $\varepsilon = 0$ and $L = 10a$ are plotted in Fig. 3, where the relation (18) is confirmed. So the topological invariant of the system can be directly detected from TOF data.

B. The PCM in the BI phase

The system is in the BI phase when $|\varepsilon| > \varepsilon_c$, in which pairwise Weyl points have been merged and become the hybrid point featuring by a hybrid spectrum

shown in Fig. 1(e). The PCM $\bar{z}(t) = 0$ because the coefficients A_z and C_z in Eq. (14) are odd function of q_z when $v_z = 0$. Then, the formula (18) is still valid and $N_w = \text{sgn}(\bar{x}\bar{y}\bar{z}) = 0$. Therefore, the topological invariants of the system in both topological trivial and non-trivial phases can be experimentally determined by directly measuring the PCM.

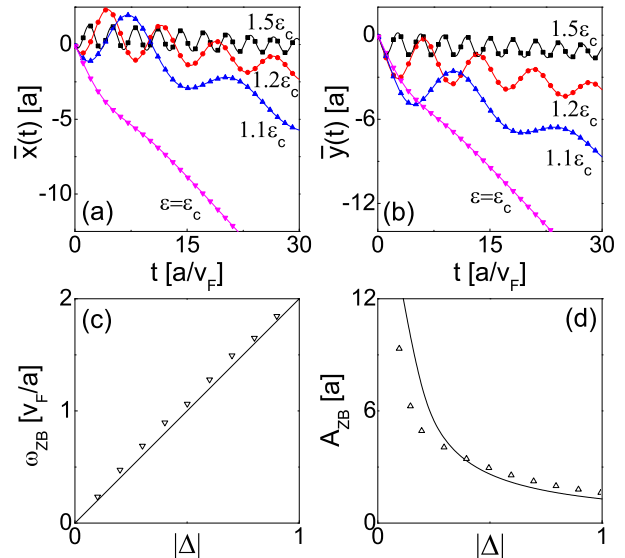


FIG. 4: (Color online). The expectation values (a) $\bar{x}(t)$ and (b) $\bar{y}(t)$ in the BI phase with different ε and $L = 10a$. The lines are obtained from Eq. (13) and the symbols are derived by the split-operator method. (c) the frequency ω_{ZB} and (d) the amplitude A_{ZB} of Zitterbewegung versus the energy gap Δ . The symbols are numerically calculated from Eq. (13) and the line of frequency (amplitude) is derived from the estimated formula $\omega_{ZB} = 2|\Delta|$ ($A_{ZB} = 1.3/|\Delta|$).

To further characterize the dynamics of the PCM in the BI phase, we plot the expectation values $\bar{x}(t)$ and $\bar{y}(t)$ with different on-site energies in Fig. 4(a,b). Periodic oscillations arise with the appearance of the gap, which is the direct evidence of ZB effect. From Eq. (13), we estimate the frequency of ZB is $\omega_{ZB} \sim 2E_{\mathbf{q}}/\hbar \sim 2|\Delta|$ and the amplitude is $A_{ZB} \sim \sqrt{B_{x,y}^2 + C_{x,y}^2} \sim 1.3/|\Delta|$. We also numerically calculate the ω_{ZB} and A_{ZB} , and the results are plotted in Fig. 4(c,d), which agree well with the estimations. At $\varepsilon = 1.2\varepsilon_c$, the amplitude A_{ZB} is about three lattice sites and the period is about $10a/v_F$, which is around 0.4 to 4.7 ms for the tunable J between 0.17 to 2.0 kHz [15, 16]. Such ZB oscillations can be readily observed in TOF experiments.

IV. CONCLUSION

In summary, we have exploited the dynamics of the Weyl quasiparticles emerged in the optical lattices where the topological WSM and trivial BI phases can be adjusted with the on-site energy. We have demonstrated

that the topological invariants and the celebrated ZB effect can be directly observed with TOF experiments. Since the dynamics of the Weyl particles could be hard to detect in a condensed matter system, our proposal in the atomic system would open up a novel possibility in research of Weyl physics.

V. ACKNOWLEDGEMENTS

We are grateful to Feng Mei and Xin Shen for useful discussions. This work was supported by the NKRPD of China (Grant No. 2016YFA0301803), the NSFC (Grants No. 11474153 and 11604103), and the PCSIRT (Grant No. IRT1243). D. W. Z. was supported by the NSF of Guangdong Province (Grant No. 2016A030313436) and the Startup Foundation of SCNU.

Z. L. and H. Q. W. contributed equally to this work.

VI. APPENDIX

A. The split-operator method

It is generally known that the final wave function after an evolution governed by the effective Hamiltonian [Eq. (6) in the main text] with time t , can be obtained as

$$\Psi(x, y, z, t) = \hat{T} \exp\left(-\frac{i}{\hbar} \int_0^t H_{\text{eff}}(t') dt'\right) \Psi(x, y, z, 0), \quad (\text{A1})$$

where \hat{T} denotes the the time ordering operator, $\Psi(x, y, z, 0)$ is the initial wave packet. The effective Hamiltonian can be expressed as the sum of operators corresponding to the kinetic and potential energies of the system in the form $\hat{H}_{\text{eff}} = \hat{T} + \hat{V}$. By using the standard split-operator method, Eq.(A1) can be rewritten as

$$\begin{aligned} \Psi(x, y, z, t + \delta t) = & \left[e^{-\frac{i}{\hbar} \hat{T} \delta t} e^{-\frac{i}{\hbar} \hat{V} \delta t} e^{-\frac{i}{\hbar} \hat{T} \delta t} + \mathcal{O}(\delta t^3) \right] \\ & \times \Psi(x, y, z, t), \end{aligned} \quad (\text{A2})$$

where $\hat{T} = \alpha_x v_x \hat{p}_x \sigma_y + \alpha_y v_y \hat{p}_y \sigma_x + (\alpha_z v_z \hat{p}_z + \frac{\hat{p}_z^2}{2m^*}) \sigma_z$, $\hat{V} = \Delta \sigma_z$. In the sufficiently short time δt , the high-order term $\mathcal{O}(\delta t^3)$ (due to noncommutation) can be safely neglected. One can connect the position and the momentum spaces by using the Fourier transform. Therefore, we can finally get the numerical solution of $\Psi_{x,y,z,t}$ following the computation procedure step by step with time step δt [38].

B. The relations among the topological numbers and the center-of-mass positions

There are eight Weyl points for the Hamiltonian H_k described in Eq. (2) in the main text. By requiring

the coefficients of the Pauli matrices to be zero, we obtain $W = [0 \text{ or } \pi, \pm \frac{\pi}{2}, \pm \arccos(\frac{-\varepsilon}{2J_z})]$. By expanding the quasi-momentum \mathbf{k} at W points, $\mathbf{k} = W + \mathbf{q}$, we have

$$\begin{aligned} \sin(k_x + q_x) &= \sin(k_x) + \cos(k_x)q_x - \frac{\sin(k_x)}{2}q_x^2 \\ &= \begin{cases} +q_x, & \text{for } k_x = 0 \\ -q_x, & \text{for } k_x = \pi \end{cases}. \end{aligned} \quad (\text{B1})$$

$$\begin{aligned} \cos(k_y + q_y) &= \cos(k_y) - \sin(k_y)q_y - \frac{\cos(k_y)}{2}q_y^2 \\ &= \begin{cases} -q_y, & \text{for } k_y = \frac{\pi}{2} \\ +q_y, & \text{for } k_y = -\frac{\pi}{2} \end{cases}. \end{aligned} \quad (\text{B2})$$

$$\begin{aligned} \cos(k_z + q_z) &= \cos(k_z) - \sin(k_z)q_z - \frac{\cos(k_z)}{2}q_z^2 \\ &= \begin{cases} -\frac{\varepsilon}{2J_z} - \sqrt{1 - (\frac{-\varepsilon}{2J_z})^2}q_z + \frac{\varepsilon}{2J_z} \cdot \frac{q_z^2}{2}, & \text{for } k_z = +\arccos\frac{-\varepsilon}{2J_z} \\ -\frac{\varepsilon}{2J_z} + \sqrt{1 - (\frac{-\varepsilon}{2J_z})^2}q_z + \frac{\varepsilon}{2J_z} \cdot \frac{q_z^2}{2}, & \text{for } k_z = -\arccos\frac{-\varepsilon}{2J_z} \end{cases}. \end{aligned} \quad (\text{B3})$$

Substituting them in Eq. (2), we obtain the effective Hamiltonian (6). In the WSM phase, there exists a one-to-one correspondence between the sign $(\alpha_x, \alpha_y, \alpha_z)$ and the location of a Weyl point (k_x, k_y, k_z) . The relations are summed up in the Table I.

(k_x, k_y, k_z)	$(\alpha_x, \alpha_y, \alpha_z)$	N_w	N_C	octant
$(0, +\frac{\pi}{2}, +\arccos\frac{-\varepsilon}{2J_z})$	$(-, +, +)$	-1	-1	II
$(0, +\frac{\pi}{2}, -\arccos\frac{-\varepsilon}{2J_z})$	$(-, +, -)$	+1	+1	VI
$(0, -\frac{\pi}{2}, +\arccos\frac{-\varepsilon}{2J_z})$	$(-, -, +)$	+1	+1	III
$(0, -\frac{\pi}{2}, -\arccos\frac{-\varepsilon}{2J_z})$	$(-, -, -)$	-1	-1	VII
$(\pi, +\frac{\pi}{2}, +\arccos\frac{-\varepsilon}{2J_z})$	$(+, +, +)$	+1	+1	I
$(\pi, +\frac{\pi}{2}, -\arccos\frac{-\varepsilon}{2J_z})$	$(+, +, -)$	-1	-1	V
$(\pi, -\frac{\pi}{2}, +\arccos\frac{-\varepsilon}{2J_z})$	$(+, -, +)$	-1	-1	IV
$(\pi, -\frac{\pi}{2}, -\arccos\frac{-\varepsilon}{2J_z})$	$(+, -, -)$	+1	+1	VIII

TABLE I: The relations among the locations of Weyl points, the signs of Fermi velocity, winding number, Chern number and the center-of-mass' position.

In the BI phase $v_z = 0$, the sign parameter $\alpha_z = 0$. It corresponds to the topological trivial state with winding number $N_w = N_C = 0$. Therefore, we obtain that

$$\text{sgn}(\bar{x}\bar{y}\bar{z}) = \text{sgn}(\alpha_x\alpha_y\alpha_z) = \begin{cases} \pm 1, & \text{for WSM} \\ 0, & \text{for BI} \end{cases}. \quad (\text{B4})$$

C. Derivation of the Berry curvature

For the Hamiltonian (6) in the main text, the Berry curvature is given by [27],

$$\Omega_{ij} = \frac{1}{2g^3} \epsilon_{abc} g_a \partial_i g_b \partial_j g_c. \quad (\text{C1})$$

It is straightforward to derive the following results

$$\begin{aligned} \Omega_{xy} &= \frac{1}{2g^3} \epsilon_{abc} g_a \partial_x g_b \partial_y g_c = \frac{1}{2g^3} (-g_3 \partial_x g_2 \partial_y g_1) \\ &= -(\Delta + \alpha_z v_z \hbar q_z + \frac{\hbar^2 q_z^2}{2m^*}) \frac{\alpha_x \alpha_y \hbar^2 v_x v_y}{2g^3} \\ &= \begin{cases} -\frac{\alpha_x \alpha_y \alpha_z \hbar^3 v_x v_y v_z}{2g^3} q_z, & \text{for WSM} \\ -(\Delta + \frac{\hbar^2 q_z^2}{2m^*}) \frac{\alpha_x \alpha_y \hbar^2 v_x v_y}{2g^3}, & \text{for BI} \end{cases}, \end{aligned} \quad (\text{C2})$$

$$\begin{aligned} \Omega_{yz} &= \frac{1}{2g^3} \epsilon_{abc} g_a \partial_y g_b \partial_z g_c = \frac{1}{2g^3} (-g_2 \partial_y g_1 \partial_z g_3) \\ &= -q_x (\alpha_z v_z \hbar + \frac{\hbar^2 q_z}{m^*}) \frac{\alpha_x \alpha_y \hbar^2 v_x v_y}{2g^3} \\ &= \begin{cases} -\frac{\alpha_x \alpha_y \alpha_z \hbar^3 v_x v_y v_z}{2g^3} q_x, & \text{for WSM} \\ -(\frac{\hbar^2 q_z q_x}{m^*}) \frac{\alpha_x \alpha_y \hbar^2 v_x v_y}{2g^3}, & \text{for BI} \end{cases}, \end{aligned} \quad (\text{C3})$$

$$\begin{aligned} \Omega_{zx} &= \frac{1}{2g^3} \epsilon_{abc} g_a \partial_z g_b \partial_x g_c = \frac{1}{2g^3} (-g_1 \partial_z g_3 \partial_x g_2) \\ &= -q_y (\alpha_z v_z \hbar + \frac{\hbar^2 q_z}{m^*}) \frac{\alpha_x \alpha_y \hbar^2 v_x v_y}{2g^3} \\ &= \begin{cases} -\frac{\alpha_x \alpha_y \alpha_z \hbar^3 v_x v_y v_z}{2g^3} q_y, & \text{for WSM} \\ -(\frac{\hbar^2 q_z q_y}{m^*}) \frac{\alpha_x \alpha_y \hbar^2 v_x v_y}{2g^3}, & \text{for BI} \end{cases}, \end{aligned} \quad (\text{C4})$$

Then we have the general expression of Berry curvature in the process of Weyl points' merging

$$\begin{aligned} \Omega &= -\frac{\alpha_x \alpha_y \hbar^2 v_x v_y}{2E_{\mathbf{q}}^3} (\alpha_z v_z \hbar k_x + \frac{\hbar^2 k_z k_x}{m^*}, \alpha_z v_z \hbar k_y \\ &\quad + \frac{\hbar^2 k_z k_y}{m^*}, \Delta + \alpha_z v_z \hbar k_z + \frac{\hbar^2 k_z^2}{m^*}). \end{aligned} \quad (\text{C5})$$

By tuning the parameter Δ [see Eq. (C5)], one can obtain the corresponding Berry curvature in the whole process of topological phase transition. We get, for the standard Weyl point,

$$\Omega = -sgn(\alpha_x \alpha_y \alpha_z) \hbar^3 v_x v_y v_z \mathbf{q} / (2E_{\mathbf{q}}^3), \quad (\text{C6})$$

and for the hybrid point,

$$\Omega = -\frac{\alpha_x \alpha_y \hbar^4 v_x v_y}{2m^* E_{\mathbf{q}}^3} (k_x k_z, k_y k_z, \frac{\Delta m^*}{\hbar^2} + \frac{k_z^2}{2}). \quad (\text{C7})$$

Thus, by integrating the whole sphere surrounding a Weyl/hybrid point, one can easily obtain the corresponding Chern number.

- [1] H. Weyl, Z. Phys. **56**, 330 (1929).
[2] L. Balents, Physics **4**, 36 (2011); F. Wilczek, Phys. Today **51**, 11 (1998).
[3] X. Wan, A. M. Turner, A. Vishwannath, and S. Y. Savrasov, Phys. Rev. B **83**, 205101 (2011).
[4] G. Xu, H. Weng, Z. Wang, X. Dai, and Z. Fang, Phys. Rev. Lett. **107**, 186806 (2011).
[5] A. A. Burkov and L. Balents, Phys. Rev. Lett. **107**, 127205 (2011).
[6] L. Lu, L. Fu, J. D. Joannopoulos, M. Soljačić, Nat. Photonics **7**, 294 (2013).
[7] L. Lu, J. D. Joannopoulos, M. Soljačić, Nat. Photonics **8**, 821 (2014).
[8] S. -Y. Xu, I. Belopolski, N. Alidoust, M. Neupane, G. Bian, C. Zhang, R. Sankar, G. Chang, Z. Yuan, C. C. Lee, S. M. Huang, H. Zheng, J. Ma, D. S. Sanchez, B. Wang, A. Bansil, F. Chou, Pavel P. Shibayev, H. Lin, S. Jia, M. Z. Hasan, Science **349**, 613 (2015).
[9] B. Q. Lv, H. M. Weng, B. B. Fu, X. P. Wang, H. Miao, J. Ma, P. Richard, X. C. Huang, L. X. Zhao, G. F. Chen, Z. Fang, X. Dai, T. Qian, and H. Ding Phys. Rev. X **5**, 031013 (2015).
[10] L. Lu, Z. Wang, D. Ye, L. Ran, L. Fu, J. D. Joannopoulos, and Marin Soljačić, Science **349** 622 (2015).
[11] T. Dubček, C. J. Kennedy, L. Lu, W. Ketterle, M. Soljačić and H. Buljan, Phys. Rev. Lett. **114**, 225301 (2015).
[12] W. -Y. He, S. Z. Zhang and K. T. Law, arXiv:1501.02348.
[13] Y. Xu and C. Zhang, arXiv:1510.03355.
[14] D. W. Zhang, S. -L. Zhu and Z. D. Wang, Phys. Rev. A **92**, 013632 (2015).
[15] M. Aidelsburger, M. Atala, M. Lohse, J. T. Barreiro, B. Paredes, and I. Bloch, Phys. Rev. Lett. **111**, 185301 (2013).
[16] M. Aidelsburger, M. Atala, S. Nascimbene, S. Trotzky, Y.-A. Chen, and I. Bloch, Appl. Phys. B, **113**, 1 (2013).
[17] H. Miyake, G. A. Siviloglou, C. J. Kennedy, W. C. Burton, and W. Ketterle, Phys. Rev. Lett. **111**, 185302

- (2013).
- [18] S. -L. Zhu, B. -G. Wang, and L. -M. Duan, *Phys. Rev. Lett.* **98**, 260402 (2007).
- [19] J. M. Hou, W. X. Yang, and X. J. Liu, *Phys. Rev. A* **79**, 043621 (2009).
- [20] D. W. Zhang, Z. D. Wang and S. -L. Zhu, *Frontiers of Physics* **7**, 31 (2012).
- [21] P. Dietl, F. Piéchon, and G. Montambaux, *Phys. Rev. Lett.* **100**, 236405 (2008).
- [22] M. O. Goerbig, J.-N. Fuchs, G. Montambaux, and F. Piéchon, *Phys. Rev. B* **78**, 045415 (2008)
- [23] N. Goldman, A. Kubasiak, A. Bermudez, P. Gaspard, M. Lewenstein, and M. A. Martin-Delgado, *Phys. Rev. Lett.* **103**, 035301 (2009).
- [24] L. Tarruell, D. Greif, T. Uehlinger, G. Jotzu, and T. Esslinger, *Nature (London)* **483**, 302 (2012).
- [25] K. K. Gomes, W. Mar, W. Ko, F. Guinea, and H. C. Manoharan, **483**, 306 (2012).
- [26] L. Duca, T. Li, M. Reitter, I. Bloch, M. Schleier-Smith, and U. Schneider, *Science* **347**, 288 (2015).
- [27] G. E. Volovik, *The Universe in a Helium Droplet* (Oxford University Press, Oxford, 2003).
- [28] D. Xiao, M. C. Chang, and Q. Niu, *Rev. Mod. Phys.* **82**, 1959 (2010).
- [29] N. Nagaosa, J. Sinova, S. Onoda, A. H. MacDonald, and N. P. Ong, *Rev. Mod. Phys.* **82**, 1539 (2010).
- [30] J. Y. Vaishnav and C. W. Clark, *Phys. Rev. Lett.* **100**, 153002 (2008).
- [31] L. J. LeBlanc, M. C. Beeler, K. Jimenez-Garcia, A. R. Perry, S. Sugawa, R. A. Williams, I. B. Spielman, *New J. Phys.* **15**, 073011 (2013).
- [32] C. Qu, C. Hamner, M. Gong, C. Zhang, and P. Engels, *Phys. Rev. A* **88**, 021604(R) (2013).
- [33] Z. Li, H. Cao and L. B. Fu, *Phys. Rev. A* **91**, 023623 (2015).
- [34] S. Ghosh and A. Manchon, arXiv:1605.02207.
- [35] W. Zawadzki and T. M. Rusin, *J. Phys.: Condens. Matter* **23** 143201 (2011).
- [36] E. Romera and F. de los Santos, *Phys. Rev. B* **80**, 165416 (2009),
- [37] V. Ya. Demikhovskii, G. M. Maksimova, A. A. Perov, and A. V. Telezhnikov, *Phys. Rev. A* **85**, 022105 (2012).
- [38] H. F. Trotter, *Proc. Amer. Math. Soc.* **10**, 545 (1959); H. De Raedt, *Comput. Phys. Rep.* **7**, 1 (1987); *Europhys. Lett.* **3**, 139 (1987); M. Suzuki, *Phys. Lett. A* **146**, 319 (1990).